AIAA JOURNAL
Vol. 41, No. 2, February 2003

Lumped Element Modeling of Piezoelectric-Driven Synthetic Jet Actuators

Quentin Gallas,* Ryan Holman,* Toshikazu Nishida,† Bruce Carroll,‡ Mark Sheplak,§ and Louis Cattafesta¶
University of Florida, Gainesville, Florida 32611-6250

A lumped element model of a piezoelectric-driven synthetic-jet actuator is presented. A synthetic jet, also known as a zero net mass-flux device, uses a vibrating diaphragm to generate an oscillatory flow through a small orifice or slot. In lumped element modeling, the individual components of a synthetic jet are modeled as elements of an equivalent electrical circuit using conjugate power variables. The frequency-response function of the circuit is derived to obtain an expression for Q_{out}/V_{ac}, the volume flow rate through the orifice per applied voltage across the piezoceramic. The circuit is analyzed to provide physical insight into the dependence of the device behavior on geometry and material properties. Methods to estimate the model parameters are discussed, along with pertinent model assumptions, and experimental verification is presented of the lumped parameter models. In addition, two prototypical synthetic jet actuators are built and tested. Very good agreement is obtained between the predicted and measured frequency-response functions.

I. Introduction

SYNTHETIC-JET actuators have been the focus of significant research activity for the past decade.[1] The interest in synthetic jets is primarily due to their utility in flow control applications, such as separation control, mixing enhancement, etc.[2–6] A schematic of a synthetic-jet actuator is shown in Fig. 1. A typical synthetic jet, also known as a zero net mass-flux device, uses a vibrating diaphragm to drive oscillatory flow through a small orifice or slot. Although there is no source, a mean jet flow is established a few diameters from the orifice due to the entrained fluid.

In addition to studies that emphasize applications, there are numerous others that have concentrated on the design, visualization, and/or measurements of synthetic jets.[7–10] Several computational studies also have focused on fundamental aspects of these devices.[11–14] Crook and Wood[9] emphasize the importance of understanding the scaling and operational characteristics of a synthetic jet. Clearly, this information is required to design an appropriate device for a particular application. In addition, feedback control applications require the actuator transfer function that relates the input voltage to the output property of interest, for example, volumetric flow rate, momentum, etc., in the control system.

The synthetic jet represents a coupled electromechanical-acoustic system with frequency-dependent properties determined by device dimensions and material properties. The analysis and design of coupled-domain transducer systems are commonly performed using lumped element models.[15–17]

The main assumption employed in lumped element modeling (LEM) is that the characteristic length scales of the governing physical phenomena are much larger than the largest geometric dimension. For example, in an acoustic system, the acoustic wavelength must be significantly larger than the device itself. If this assumption holds, then the temporal and spatial variations can be decoupled, and the governing partial differential equations for the distributed system can be "lumped" into a set of coupled ordinary differential equations. This approach provides a simple method to estimate the low-frequency dynamic response of a system for design and control-system implementation.

The purpose of this paper is the rigorous study of the application of LEM to piezoelectric-driven synthetic-jet actuators. To the authors' knowledge, this paper represents the first application of LEM to piezoelectric-driven synthetic jets. McCormick[18] employed LEM to a speaker-driven synthetic jet to relate the voltage input to the output volume velocity of the actuator. Rathnasingham and Breuer[19] were the first to develop a low-order model of a synthetic jet, using a control-volume model for the flow and an empirical model for the structural dynamics of the diaphragm. In this paper, the various lumped elements for each component of a synthetic jet are developed theoretically. The resulting equivalent circuit is then analyzed to understand the effects of geometry and material properties on important design parameters, such as resonance frequency and volume displacement per applied voltage. The model assumptions and limitations are discussed, along with the results of experiments designed to assess the validity of this modeling approach.

II. Lumped Element Modeling

In LEM, the coupling between the various energy domains is realized by using equivalent two-port models of the physical system. An equivalent circuit model is constructed by lumping the distributed energy storage and dissipation into ideal generalized one-port circuit elements. In an electroacoustic system, differential pressure and voltage are effort variables, whereas current and volumetric flow rate are flow variables. An impedance analogy is employed, in which elements that share a common effort are connected in parallel, whereas those sharing a common flow are connected in series. For a synthetic jet, three different energy domains are involved: electrical, mechanical, and fluidic/acoustic.

The electromechanical actuator consists of an axisymmetric piezoceramic patch bonded to a clamped metal diaphragm. The composite diaphragm is driven into motion via an applied ac voltage. The primary purpose of the piezoelectric diaphragm is to produce large volume displacements to force fluid into and out of the cavity, which represents a conversion from the mechanical to the acoustofluidic energy domain. Consequently, the frequency range of the analysis is limited from dc to somewhat beyond the fundamental vibration mode of the composite diaphragm, but less than the natural frequency of any higher-order modes.[20] Linear composite plate theory is used to obtain the short-circuit pressure-deflection characteristics. Then, the diaphragm is lumped into an equivalent acoustic mass and acoustic compliance. The former represents stored kinetic energy,

Received 10 May 2002; revision received 30 August 2002; accepted for publication 30 August 2002.

*Graduate Student, Department of Mechanical and Aerospace Engineering. Student Member AIAA.
†Associate Professor, Department of Electrical and Computer Engineering.
‡Associate Professor, Department of Mechanical and Aerospace Engineering. Associate Fellow AIAA.
§Assistant Professor, Department of Mechanical and Aerospace Engineering. Member AIAA.
¶Assistant Professor, Department of Mechanical and Aerospace Engineering; catman@mae.ufl.edu. Associate Fellow AIAA.

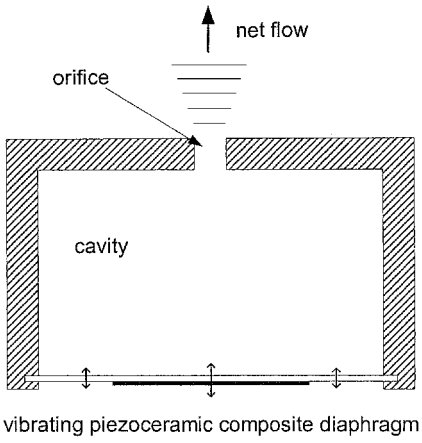

Fig. 1 Schematic of a synthetic jet.

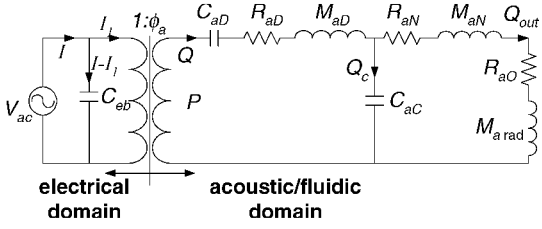

Fig. 2 Equivalent circuit representation of a piezoelectric-driven synthetic jet.

and the latter models stored potential energy. Similarly, the electromechanical transduction characteristics are determined by the unloaded or "free" voltage-deflection characteristics. The piezoelectric electromechanical coupling is lumped into an effective acoustic piezoelectric coefficient.

In general, the cavity contains a compressible gas that stores potential energy and is, therefore, modeled as an acoustic compliance. Viscous effects in the orifice dissipate a portion of the kinetic energy stored in the motion of the oscillating fluid mass. Therefore, there will be an effective acoustic mass and acoustic resistance associated with the orifice neck. Flow through the orifice produces losses associated with the discharge of flow from the jet exit. An acoustic radiation impedance must also be added if the fluid is ejected into a semi-infinite medium.

The equivalent circuit representation for the synthetic jet is shown in Fig. 2. In the notation that follows, the first subscript denotes the domain, for example, *a* for acoustic and *e* for electric, and the second subscript describes the element, for example, *D* for diaphragm. In the electrical domain, C_{eb} is the blocked electrical capacitance of the piezoelectric diaphragm driven by an ac voltage V_{ac}. The term blocked is used because it is the impedance seen by the source when the diaphragm motion is prevented. Although not shown here, a resistor can be introduced in series or in parallel with C_{eb} to represent the dielectric loss in the piezoceramic (Ref. 17, p. 358).

The compliance, mass, and damping of the piezoelectric diaphragm are normally represented in the mechanical domain, but the acoustic equivalent elements are used for simplicity here to avoid the use of ambiguous reference areas to convert from mechanical to acoustic impedance (Ref. 17, p. 266). In particular, C_{aD} and M_{aD} are the short-circuit effective acoustic compliance and mass of the piezoceramic composite diaphragm, respectively, and R_{aD} is the structural damping in the acoustic domain. The term short circuit is used because the preceding parameters correspond to the condition when the piezoelectric patch is electrically shorted. Also, a radiation impedance must be included if the back side of the diaphragm is radiating into an open medium. C_{aC} is the acoustic compliance of the cavity, whereas R_{aN} and M_{aN} are the acoustic resistance and mass of the fluid in the neck, respectively. Finally, R_{aO} is the nonlinear resistance associated with the orifice discharge, and $M_{a\,\text{rad}}$ is the acoustic radiation mass of the orifice.

In this paper, it is assumed that the synthetic jet exhausts into a semi-infinite ambient air medium and that the diaphragm is not subject to a mean differential pressure. If necessary, a vent channel can be used to equilibrate the mean static pressure across the diaphragm, in a manner similar to a microphone.[21] For simplicity, it is assumed that there is no grazing flow, and compressibility effects in the orifice are neglected.

The structure of the equivalent circuit is explained as follows. An ac voltage V_{ac} is applied across the piezoceramic to create an effective acoustic pressure that drives the diaphragm into motion. This represents a conversion from the electrical to the acoustic domain (bypassing the mechanical domain via integration to produce a volume displacement) and is accounted for via a transformer possessing a turns ratio ϕ_a (in pascal per volt). An ideal transformer converts energy from one domain to another without losses and obeys the relations

$$I_1 = \phi_a Q, \qquad V_{\text{ac}} = P/\phi_a \tag{1}$$

In addition, a transformer converts an electrical impedance Z_e to an acoustic impedance Z_a via

$$Z_e = V_{\text{ac}}/I_1 = (P/\phi_a)/\phi_a Q = (P/Q)\big/\phi_a^2 = Z_a\big/\phi_a^2 \tag{2}$$

The motion of the diaphragm either can compress the fluid in the cavity or can eject/ingest fluid through the orifice. Physically, this is represented as a volume velocity divider, $Q = Q_c + Q_{\text{out}}$. The goal of the design is to maximize the magnitude of the volume flow rate through the orifice per applied voltage $|Q_{\text{out}}/V_{\text{ac}}|$.

III. Equivalent Circuit Model Analysis

Before estimating the lumped parameters defined earlier, it is instructive to analyze the equivalent circuit to obtain the frequency-response function $Q_{\text{out}}(s)/V_{\text{ac}}(s)$, where $s = j\omega$. By the use of Eq. (2), the transformer can be eliminated by converting each of the acoustic impedances to their electrical equivalent. The result is depicted in Fig. 3, where

$$Z_{eD}(s) = \left(1\big/\phi_a^2\right)(R_{aD} + sM_{aD} + 1/sC_{aD})$$

$$Z_{eC}(s) = \left(1\big/\phi_a^2\right)(1/sC_{aC})$$

$$Z_{eO}(s) = [(R_{aN} + R_{aO}) + s(M_{aN} + M_{a\,\text{rad}})]\big/\phi_a^2 \tag{3}$$

are the electric impedance of the diaphragm, cavity, and orifice, respectively. Substituting in the expressions for Z_{eD}, Z_{eC}, and Z_{eO} and grouping powers of s in the numerator and denominator results in

$$\frac{Q_{\text{out}}(s)}{V_{\text{ac}}(s)} = \frac{\phi_a C_{aD} s}{a_4 s^4 + a_3 s^3 + a_2 s^2 + a_1 s + 1} \tag{4}$$

where

$$a_1 = C_{aD}(R_{aO} + R_{aN} + R_{aD}) + C_{aC}(R_{aO} + R_{aN})$$

$$a_2 = C_{aD}(M_{a\,\text{rad}} + M_{aN} + M_{aD}) + C_{aC}(M_{a\,\text{rad}} + M_{aN}) + C_{aC}C_{aD}R_{aD}(R_{aO} + R_{aN})$$

$$a_3 = C_{aC}C_{aD}[M_{aD}(R_{aO} + R_{aN}) + (M_{a\,\text{rad}} + M_{aN})R_{aD}]$$

$$a_4 = C_{aC}C_{aD}M_{aD}(M_{a\,\text{rad}} + M_{aN}) \tag{5}$$

Although this expression is somewhat complicated, it reveals some important features without having to estimate any of the parameters in Eq. (5). For this discussion, these parameters can be

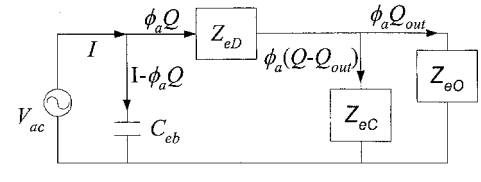

Fig. 3 Alternative equivalent circuit model.

thought of as constants, although in reality some are likely to exhibit frequency and amplitude dependence, that is, due to nonlinear effects. For a dc voltage ($s = 0$), the volume velocity is zero. At low frequencies ($s \to 0$), the volume velocity is proportional to $d_a V_{ac}\omega$ because the transduction factor is defined as $\phi_a = d_a/C_{aD}$, where d_a is an effective acoustic piezoelectric coefficient defined later [see Eq. (22)]. This result emphasizes the need to optimize the design of the piezoceramic composite diaphragm[20] and also indicates that Q_{out} and V_{ac} are 90 deg out of phase at low frequencies.

At high frequencies ($s \to \infty$), Eq. (4) becomes

$$Q_{out}/V_{ac} = d_a \Big/ C_{aC} C_{aD} M_{aD} (M_{aN} + M_{a\,rad}) s^3 \tag{6}$$

The output, therefore, decreases at a rate of 60 dB/decade and is inversely proportional to the product of the masses and compliances in the system.

The denominator in Eq. (4) is a fourth-order polynomial in s, indicating two resonance frequencies. A compact analytical expression for the two resonance frequencies is desirable. The first and second resonance frequencies, f_1 and f_2, are controlled by, but are not identical to, the short-circuit piezoelectric diaphragm natural frequency,

$$f_D = (1/2\pi)\sqrt{1/M_{aD}C_{aD}} \tag{7}$$

and the Helmholtz resonator frequency,

$$f_H = (1/2\pi)\sqrt{1/(M_{aN} + M_{a\,rad})C_{aC}} \tag{8}$$

with the constraint that

$$f_1 f_2 = f_D f_H \tag{9}$$

The measure of the coupling of a system is a function of the mass or compliance ratio.[15] When small damping is assumed, the denominator in Eq. (4) yields the following relationship between the natural frequencies:

$$\left[\left(f_2^2 - f_D^2\right) + \left(f_1^2 - f_H^2\right)\right] \Big/ f_H^2 = [(M_{aN} + M_{a\,rad})/M_{aD}] = \alpha \tag{10}$$

where α is defined as the ratio of the orifice masses to the diaphragm mass. Similarly, a compliance ratio β can be defined as

$$\left[\left(f_2^2 - f_D^2\right) + \left(f_1^2 - f_H^2\right)\right] \Big/ f_D^2 = C_{aD}/C_{aC} = \beta \tag{11}$$

Given the compliance ratio, which is usually easier to estimate, one can obtain the following quadratic formula for $\psi = f_i^2$:

$$\psi^2 - \left[f_D^2(1+\beta) + f_H^2\right]\psi + f_D^2 f_H^2 = 0 \tag{12}$$

The two roots of Eq. (9) are the square of the natural frequencies of the synthetic jet, f_1^2 and f_2^2. In the next section, two important cases are examined to gain physical insight into the behavior of the device under different limiting conditions.

A. Case 1: Incompressible Limit $1/\beta = C_{aC}/C_{aD} \to 0$

If it is assumed that the fluid is an isentropic, ideal gas, the acoustic cavity compliance is obtained from the cavity volume V_0, gas density ρ_0, and the isentropic speed of sound c_0 via

$$C_{aC} = V_0 \Big/ \rho_0 c_0^2 \tag{13}$$

In practice, $C_{aC}/C_{aD} \to 0$ is achieved by minimizing the cavity volume or operating in a liquid medium.

Because the coefficients a_3 and a_4 in Eq. (5) are both proportional to C_{aC}, the synthetic-jet transfer function reduces to the second-order system,

$$\frac{Q_{out}(s)}{V_{ac}(s)} = \frac{(d_a/a_2')s}{s^2 + (a_1'/a_2')s + 1/a_2'} \tag{14}$$

where the prime denotes the limit with $C_{aC}/C_{aD} \to 0$.

The denominator in Eq. (14) is written in the form of a canonical second-order system, $s^2 + 2\zeta\omega_n s + \omega_n^2$. By inspection, the natural frequency and damping ratio for the incompressible case are given by

$$\omega_{incomp} = \sqrt{1/\{C_{aD}M_{aD}[1 + (M_{aN} + M_{a\,rad})/M_{aD}]\}} \tag{15}$$

$$\zeta_{incomp} = \tfrac{1}{2}(R_{aO} + R_{aN} + R_{aD})\sqrt{C_{aD}/(M_{aN} + M_{a\,rad} + M_{aD})} \tag{16}$$

If $M_{aD} \gg M_{aN} + M_{a\,rad}$, then the natural frequency of the synthetic-jet actuator equals that of the diaphragm. At resonance, the response is proportional to the effective acoustic piezoelectric coefficient and is limited by the resistances of the circuit and the acoustic compliance of the diaphragm:

$$Q_{out}/V_{ac} = (1/C_{aD})[d_a/(R_{aO} + R_{aN} + R_{aD})] \tag{17}$$

B. Case 2: Rigid Diaphragm Limit $\beta = C_{aD}/C_{aC} \to 0$

As described by Prasad et al.,[20] the size of the piezoceramic patch is not negligible compared to the metal diaphragm for high actuation performance. Therefore, the piezoceramic composite diaphragm cannot accurately be modeled as a homogeneous circular plate. Nonetheless, if it is assumed that the diaphragm is clamped, the acoustic compliance of a homogeneous clamped circular plate provides insight into the scaling behavior of the diaphragm:

$$C_{aD} = \frac{\pi a^6 (1 - \nu^2)}{16 E h^3} \tag{18}$$

where a is the radius, E is the elastic modulus, ν is Poisson's ratio, and h is the thickness. From Eq. (18), C_{aD} decreases with decreasing thickness ratio a/h and increasing elastic modulus.

As in the earlier case, the coefficients a_3 and a_4 in Eq. (5) are zero, and the synthetic-jet transfer function reduces to a second-order system. The limit $C_{aD}/C_{aC} \to 0$ leads to the following expressions for the natural frequency, damping ratio, and response at resonance:

$$\omega_{stiff} = \sqrt{1/(M_{aN} + M_{a\,rad})C_{aC}} \tag{19}$$

$$\zeta_{stiff} = \tfrac{1}{2}(R_{aO} + R_{aN})\sqrt{C_{aC}/(M_{a\,rad} + M_{aN})} \tag{20}$$

$$Q_{out}/V_{ac} = (1/C_{aC})[d_a/(R_{aO} + R_{aN})] \tag{21}$$

In this case, the natural frequency of the jet corresponds to the resonant frequency of the Helmholtz resonator. At resonance, the response is limited by the orifice flow resistances and the cavity compliance. By comparison with Eq. (17), the resonant response differs for these cases by the ratio of the acoustic compliances and by the contribution of the acoustic resistance of the diaphragm in the incompressible case.

C. Model Parameter Estimation

In this section, the methods and assumptions used to estimate each of the quantities in Eq. (5) are outlined. See Refs. 16, 17, and 22 for details of the methodology. The details of the two-port model for the piezoceramic plate can be found in Ref. 20.

The piezoelectric diaphragm vibrates in response to both an applied ac voltage and oscillatory differential pressure according to the relation

$$Q = j\omega(d_a V_{ac} + C_{aD} P) \tag{22}$$

where $d_a = |(Q/j\omega V_{ac})|_{P=0}$ is defined as the effective acoustic piezoelectric coefficient that relates the volume velocity Q of the diaphragm to the applied voltage V_{ac}, and $C_{aD} = (Q/j\omega P)|_{V_{ac}=0} = (\Delta\ \text{volume}/P)|_{V_{ac}=0}$ is the short-circuit acoustic compliance that relates an applied differential pressure to the volume displacement of the diaphragm.

The vertical deflection $w(r)$ due to an applied differential pressure is lumped into an equivalent acoustic mass M_{aD} by equating the lumped kinetic energy of the vibrating diaphragm to the total kinetic energy using

$$\frac{1}{2} M_{aD} Q^2 = \int_0^a \frac{\rho''(r)}{2} \dot{w}(r)^2 2\pi r \, dr \tag{23}$$

where $\rho''(r)$ is the distributed mass per unit area, Q is the net volume velocity of the diaphragm, a is the radius of the diaphragm, and $\dot{w}(r) = j\omega w(r)$ is the distributed vertical velocity. All of these parameters are calculated via linear composite plate theory. (See Ref. 20 for details.) The acoustic resistance R_{aD} represents the losses due to damping effects in the diaphragm and is given by

$$R_{aD} = 2\zeta\sqrt{M_{aD}/C_{aD}} \tag{24}$$

where ζ is the damping coefficient that is determined experimentally.

The blocked electrical capacitance C_{eb} in Fig. 2 is related to the free electrical capacitance of the piezoceramic $C_{\text{ef}} = \varepsilon A_p / h_p$ by

$$C_{\text{eb}} = C_{\text{ef}}(1-\kappa^2) = C_{\text{ef}}\left(1 - d_a^2 \big/ C_{\text{ef}} C_{asD}\right) \tag{25}$$

where κ^2 is the electroacoustic coupling factor, ε is the dielectric constant, A_p is the piezoceramic area, and h_p is the thickness of the piezoceramic patch. However, C_{eb} does not appear in Eq. (4) and is, therefore, not required for the present analysis. Also note that the piezoceramic dielectric properties play a major role in determining the electric power requirements of the actuator.

The acoustic impedance of the cavity is given by

$$Z_{aC} = \rho_0 c_0 \cot(kD)/jS \tag{26}$$

where D is the depth, $k = \omega/c_0$ is the acoustic wave number, and S is the cross-sectional area of the cavity. Because $kD \ll 1$, the Maclaurin series is truncated after the first term to yield (see Ref. 23)

$$Z_{aC} \cong \rho_0 c_0^2 \big/ j\omega SD = \rho_0 c_0^2 \big/ j\omega V_0 = 1/j\omega C_{aC} \tag{27}$$

At low frequencies, the acoustic resistance of the neck is obtained assuming fully developed laminar pipe flow in the neck of length L and radius a_0:

$$R_{aN} = \Delta P_{\text{out}}/Q_{\text{out}} = 8\mu L/\pi a_0^4 \tag{28}$$

where μ is the viscosity of the fluid and Q_{out} is the volume flow rate produced by the differential pressure ΔP_{out}. By the use of the same assumption of fully developed pipe flow, the acoustic mass in the neck is obtained by integrating the distributed kinetic energy and equating it to the lumped kinetic energy in the acoustic domain:

$$\frac{1}{2}\rho_0 L \int_0^{a_0} u_0^2 \left[1 - \left(\frac{r}{a_0}\right)^2\right]^2 2\pi r \, \mathrm{d}r = \frac{1}{2} M_{aN} Q_{\text{out}}^2 \tag{29}$$

where u_0 is the centerline velocity that is related to the volume flow rate by $Q_{\text{out}} = u_0 \pi a_0^2/2$. The solution of Eq. (29) yields the effective acoustic mass

$$M_{aN} = 4\rho_0 L \big/ 3\pi a_0^2 \tag{30}$$

The acoustic radiation mass $M_{a\,\text{rad}}$ can be modeled for $ka_0 < 0.5$ as a piston in an infinite baffle if the circular orifice is mounted in a plate that is much larger in extent than the orifice[22]:

$$M_{a\,\text{rad}} = 8\rho_0 \big/ 3\pi^2 a_0 \tag{31}$$

The acoustic resistance associated with the discharge from the orifice can be approximated by modeling the orifice as a generalized Bernoulli flow meter (see Refs. 18 and 24):

$$R_{aO} = \frac{\frac{1}{2}K_D \rho_0 \bar{u}}{\pi a_0^2} = \frac{\frac{1}{2}K_D \rho_0 Q_{\text{out}}}{\pi^2 a_0^4} \tag{32}$$

where $\bar{u}$ is the mean velocity and K_D (assumed to be unity here) is a nondimensional loss coefficient that is a function of orifice geometry, Reynolds number, and frequency. Note that R_{aO} is a function of the volume flow rate Q_{out} through the orifice and, thereby, represents a nonlinear resistance, necessitating an iterative solution of Eq. (4).

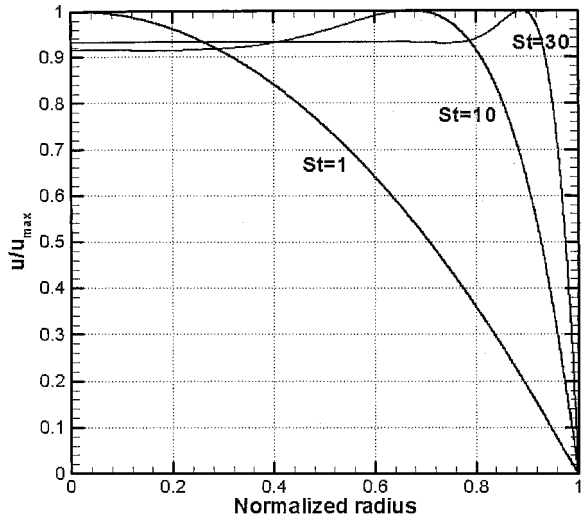

Fig. 4 Variation in velocity profile vs St = 1, 10, and 30 for oscillatory channel flow in a circular duct.

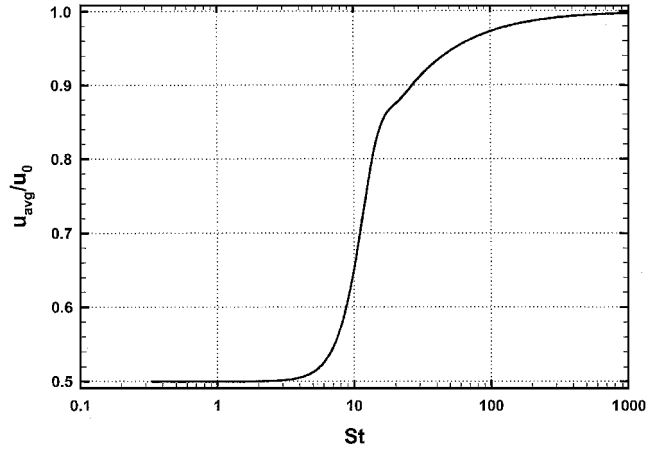

Fig. 5 Ratio of average velocity to centerline velocity vs St for oscillatory channel flow in a circular duct.

At higher frequencies, the velocity profile in the orifice is modeled as flow in a circular duct driven by an oscillating pressure gradient. The solution is given by White[25] as

$$u(r,t) = j\frac{\Delta P_{\text{out}}}{\omega\rho_0 L}\left\{1 - \frac{J_0\left[\sqrt{-j(\omega r^2/\nu)}\right]}{J_0\left[\sqrt{-j\left(\omega a_0^2/\nu\right)}\right]}\right\} e^{j\omega t} \tag{33}$$

where J_0 is a Bessel function of zero order and ν is the kinematic viscosity. The velocity u is proportional to the pressure gradient and inversely proportional to $\rho_0\omega$. Furthermore, the velocity profile is characterized by the Stokes number $\text{St} = \sqrt{(\omega a_0^2/\nu)}$, as shown in Fig. 4. In the limit of $\text{St} \to 0$, the velocity profile asymptotes to Poiseuille flow. As the Stokes number increases, the thickness of the Stokes layers decreases below a_0, leading to an inviscid core surrounded by a viscous annular region. Figure 5 shows that the ratio of the average velocity to the centerline velocity, which is 0.5 for Poiseuille flow, is strongly dependant on the Stokes number. The acoustic impedance of the orifice under these assumptions is determined by directly integrating the velocity profile to obtain Q_{out} as a function of ΔP_{out}. In this case, the real (resistive) and imaginary (reactive) parts of the acoustic impedance are a function of the Stokes number:

$$\Delta P_{\text{out}}/Q_{\text{out}} = Z_{aN} = R_{aN} + jX_{aN} = R_{aN} + j\omega M_{aN} \tag{34}$$

The results shown in Fig. 6 reveal that, at low frequencies, the acoustic resistance asymptotes to the steady value given in Eq. (28) and increases gradually with frequency. However, the acoustic mass

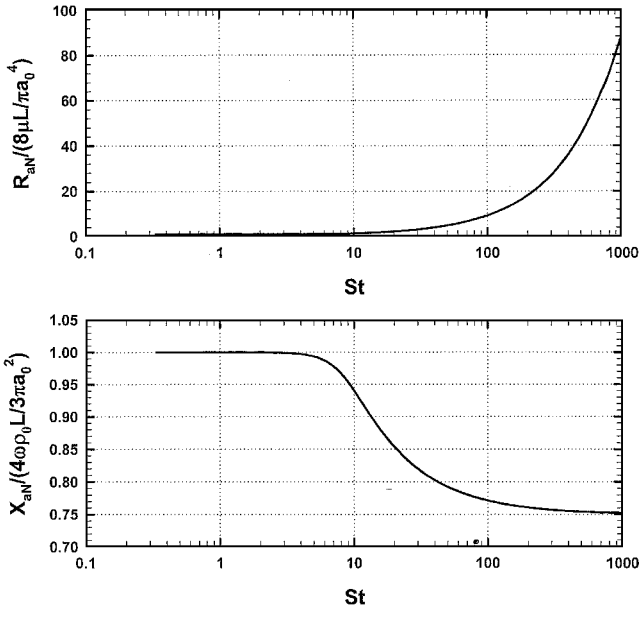

Fig. 6 Nondimensional resistance and reactance vs St for oscillatory channel flow in a circular duct.

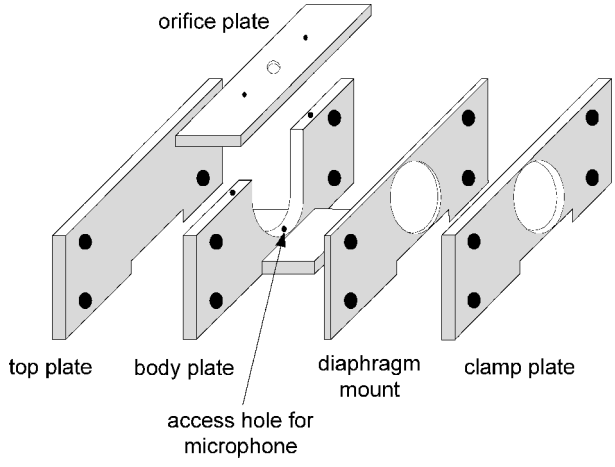

Fig. 7 Assembly diagram of modular synthetic jet.

is approximately constant with frequency. The data in Fig. 6 are used to provide frequency-dependent estimates for the acoustic resistance and mass in Eq. (4).

IV. Model Validation and Parameter Extraction

A modular piezoelectric-driven synthetic jet was constructed, as shown in Fig. 7, to perform a series of experiments to test the validity of the lumped element model parameters. The modular design permits a systematic variation of the cavity volume, orifice diameter and length, and piezoelectric diaphragm diameter and thickness. In addition, an access hole is provided for a microphone to monitor the fluctuating pressure inside the cavity.

A. Piezoelectric Transduction

The first experiment tested the linear composite plate theory that provides estimates for C_{aD}, M_{aD}, and d_a. This was accomplished by measuring the velocity of the clamped vibrating diaphragm (excited by V_{ac}) using a scanning laser vibrometer (Polytec Model PSV-200) and integrating the velocity in the frequency domain to obtain displacement. The clamped circular diaphragm was removed from the synthetic-jet apparatus and mounted on an optical table. The test was also performed in a vacuum chamber to eliminate fluid loading effects.

Figure 8 shows a comparison between the predicted and measured mode shape of the piezoceramic diaphragm to a sinusoidal excitation voltage at $f = 100$ Hz. The agreement between theory

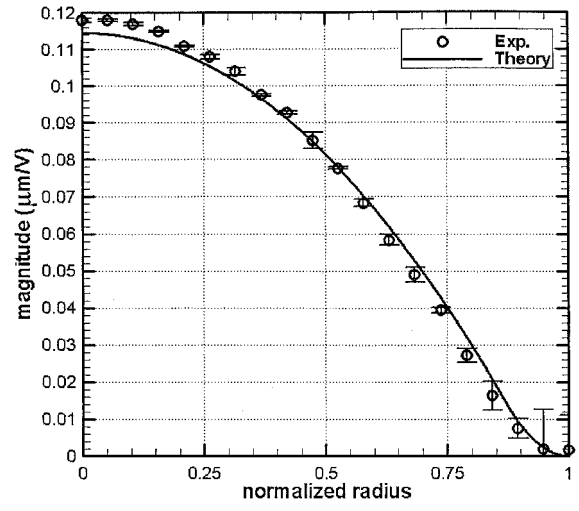

Fig. 8 Comparison between predicted and measured response of piezoceramic diaphragms to a sinusoidal excitation voltage at 100 Hz.

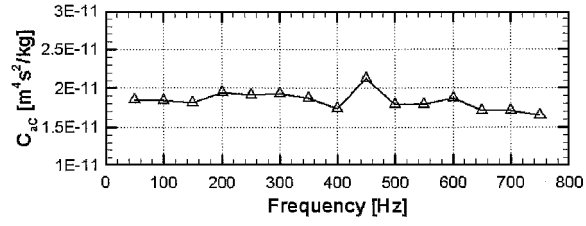

Fig. 9 Measured acoustic compliance C_{aC} vs frequency in closed cavity of synthetic jet.

and experiment is very good. The measured natural frequency of the diaphragm was 3505 Hz, whereas the computed short-circuit resonance frequency from Eq. (7) was within ~1%. Figure 8 includes random uncertainty estimates estimated from the measured response at 100 Hz, as outlined by Bendat and Piersol.[26] Key assumptions of the composite plate model, discussed in detail by Prasad et al.,[20] include a linear response, negligible bond-layer thickness and in-plane stress, and an ideal clamped boundary condition. Any violation of these assumptions will obviously degrade the accuracy of the model.

B. Cavity Acoustic Compliance

The value of the cavity acoustic compliance C_{aC} is obtained from Eq. (13). The cavity volume can be calculated from the geometry. To test the theory, the orifice was replaced with a solid cap to provide a closed cavity, and all leaks were carefully minimized. The piezoceramic was then driven with a nominal 1-V amplitude sinusoid, and the displacement of the vibrating diaphragm was measured with a laser displacement sensor (Micro-Epsilon Model ILD2000-10). A $\frac{1}{8}$-in. Brüel and Kjær (B&K) Type 4138 condenser microphone with B&K Type 2669 preamplifier measured the fluctuating pressure in the closed cavity.

The amplitude of the sinusoid was adjusted to avoid harmonics. The frequency response function between the pressure and displacement signal at the diaphragm center w_0 was used to measure P/w_0 at several frequencies and calculate C_{aC}, as shown in Fig. 9. By the use of the average measured value of 9.89 MPa/m and the measured mode shape, the cavity volume was determined to be 2.53×10^{-6} m$^3 \pm 12\%$. This nominal value is within ~1% of the cavity volume calculated from the geometry.

C. Acoustic Mass and Resistance in Orifice

The flow in the neck of the orifice is modeled via Eq. (33) as a fully developed laminar flow driven by an oscillatory pressure gradient in a circular duct of radius a_0 and length L. The data in Fig. 6 are used to provide frequency-dependent estimates for the acoustic resistance and mass in the lumped element model. Also, it has been verified that this model is in good agreement with the semi-empirical model given by Ingard[27] for the impedance of a perforated plate.

Also note that, depending on the aspect ratio L/a_0 of the orifice, the fully developed assumption may not be valid. Only for large values of L/a_0 is the fully developed assumption expected to be reasonable. For small values of L/a_0, the orifice dump loss given in Eq. (32) is expected to dominate.

The models discussed in this section are simple and neglect potentially significant issues, such as nonlinear effects due to large-amplitude pressure oscillations in the cavity[28] and transition to turbulent flow and compressibility effects in the orifice. Grazing flow effects, which are relevant when the synthetic jet interacts with a boundary layer, have also been ignored.[29]

D. Comparison Between Model and Experiment

In this section, the lumped element model is used to predict the frequency response of two synthetic-jet actuators. The dimensions and material properties of the piezoceramic diaphragms are summarized in Table 1, and the pertinent lumped element parameters are provided in Table 2. Table 3 lists the geometry of both synthetic jets.

1. *Laser Doppler Velocimetry System*

A Dantec, fiber-optic, two-component, laser doppler velocimetry system was used to measure the magnitude of the peak centerline velocity produced by a synthetic jet for varying frequency. Theatrical fog fluid was used to produce particles with a specified mean diameter of 0.35 μm. Figure 10 shows a schematic of the synthetic-jet device and the relative size of the probe volume. A 400-mm focal length, 60-mm-diam lens was used to create a probe volume size of $0.194 \times 0.194 \times 4.095$ mm with a beam half-angle of 2.718 deg. Because of the beam half-angle and the thickness of the synthetic-jet device, the minimum distance from the orifice at which velocity data could be acquired was 0.3 mm, which is less than one orifice diameter. As further evidence that the measurement location is sufficiently close to the orifice, the ratio of the measurement location to the stroke length, $x\pi f/u_{\max}(f)$, is much less than unity for the conditions tested here.[1]

2. *Data Acquisition*

Velocity data were acquired phase locked with the input actuation sinusoidal signal. As shown in Fig. 10, the probe volume length extended beyond the orifice. Therefore, the data contained many points with near zero velocity. Fortunately, these data do not affect the envelope of the phase-averaged velocity over one cycle. The maximum value was extracted from the phase-averaged velocity measurements over a range of input frequencies with $V_{ac} = 25$ V. To verify repeatability of the data, several frequencies were chosen and

Table 1 Specifications of piezoceramic diaphragms

Property	Case 1	Case 2
Shim (brass)		
Elastic modulus, Pa	8.963×10^{10}	
Poisson's ratio	0.324	
Density, kg/m^3	8700	
Thickness, mm	0.15	0.10
Diameter, mm	23.0	37.0
Piezoceramic (PZT-5A)		
Elastic modulus, Pa	6.3×10^{10}	
Poisson's ratio	0.31	
Density, kg/m^3	7700	
Thickness, mm	0.08	0.11
Diameter, mm	20.0	25.0
Relative dielectric constant	1750	
d_{31}, m/V	-1.75×10^{-10}	
C_{ef}, nF	61	76

Table 2 Calculated lumped parameters of piezoceramic diaphragms

Quantity	Case 1	Case 2
C_{aD}, s$^2 \cdot$ m^4/kg	7.39×10^{-13}	2.76×10^{-11}
M_{aD}, kg/m^4	7.669×10^3	2.289×10^3
ϕ_a, Pa/V	74.79	15.66

Table 3 Geometry of synthetic jet actuators

Property	Case 1	Case 2
	Cavity	
Volume V_0, m^3	2.50×10^{-6}	5.50×10^{-6}
	Orifice	
Radius a_0, mm	0.825	0.42
Length L, mm	1.65	0.84

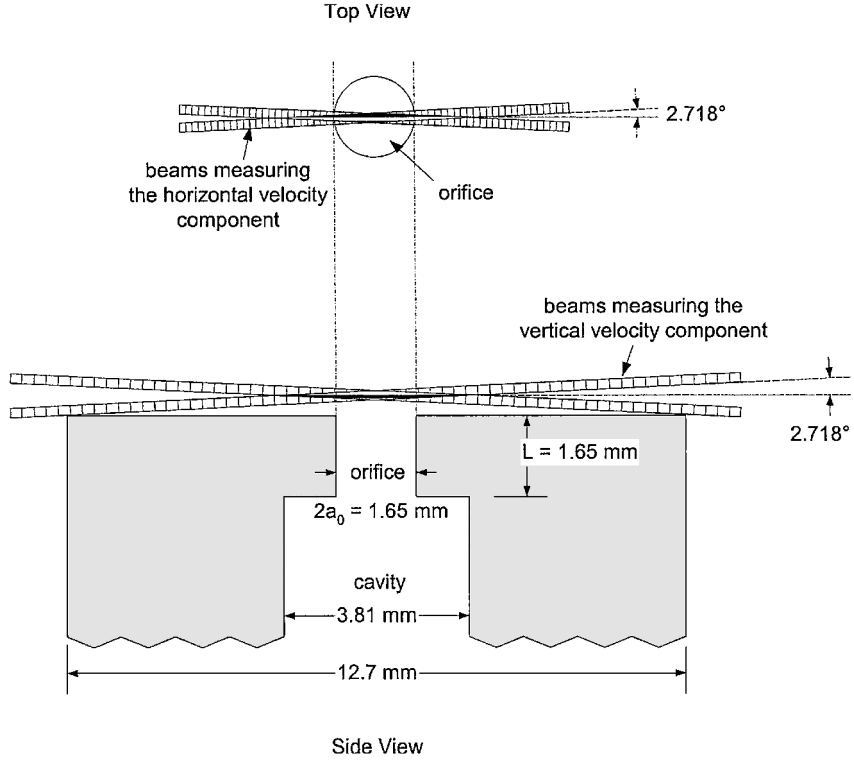

Fig. 10 Laser doppler velocimeter system setup for case 1.

Table 4 Uncertainty in maximum velocity at select frequencies for case 2

Frequency, Hz	Uncertainty in $u_{\max}(f)$, %
200	2.0
500	3.4
800	13.0

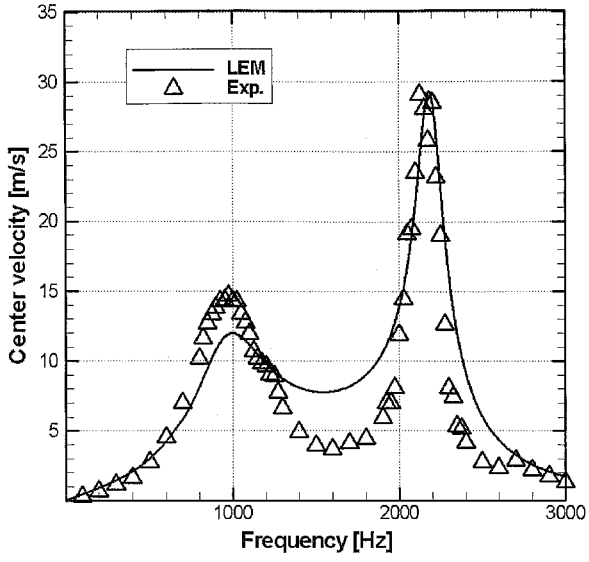

Fig. 11 Comparison between the lumped element model and experiment for case 1 ($\zeta = 0.03$ and $K_D = 1$).

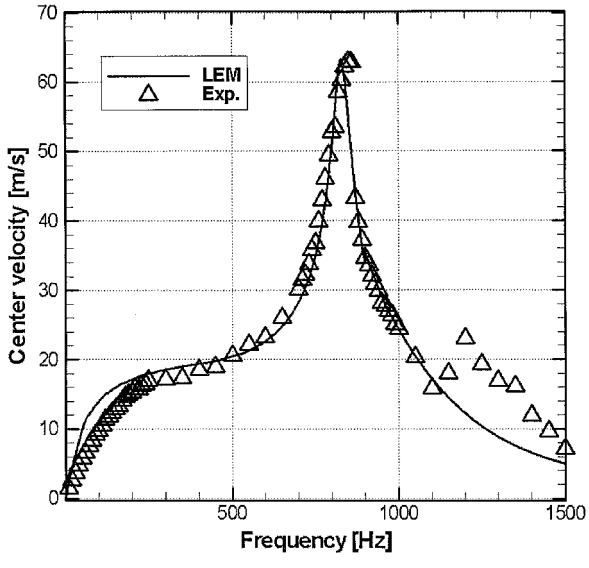

Fig. 12 Comparison between the lumped element model and experiment for case 2 ($\zeta = 0.02$ and $K_D = 1$).

velocity data were acquired over a period of several days for case 2. Table 4 summarizes the repeatability of the velocity measurements for several frequencies. Whereas the uncertainty exceeds 10% near resonance, the data are sufficiently accurate to test the validity of the lumped element model.

3. Results

As shown in Table 3, case 1 uses a smaller piezoceramic diaphragm and cavity volume and a larger orifice than case 2. However, both devices use an orifice with the same aspect ratio L/a_0 and are driven with $V_{ac} = 25$ V amplitude sinusoids. Figures 11 and 12 show the comparison between the experiment and the model just developed. The lumped element model uses Eq. (33) and Fig. 6 to model the frequency dependence of the velocity profile to determine the relationship between $u_{\max}$ and Q_{out}, which is obtained via Fig. 5. The agreement between the model and experiment in Fig. 11 is satisfactory. The main difference between the two models proposed occurs at the maximum velocity peaks, where the resistance terms dominate the system response. As shown in Table 5, the model accurately predicts the two resonance frequencies using Eq. (12).

Table 5 Comparison between lumped element model and experiment

Quantity	Source	Case 1	Case 2
f_D, Hz	Eq. (7)	2114	632
f_H, Hz	Eq. (8)	941	452
β	Eq. (11)	0.041	0.693
f_1, Hz	Eq. (12)	918	324
f_2, Hz	Eq. (12)	2167	880
f_1, Hz	Experiment	970	N/A
f_2, Hz	Experiment	2120	850

Case 2 in Fig. 12 corresponds to a case with a single dominant peak that provides jet velocities in excess of 60 m/s. The excitation voltage amplitude of 25 V corresponds to approximately 35% of the coercive or breakdown electric field strength ($\sim$1.18 V/μm) of the piezoceramic. The lumped element model accurately predicts the resonance frequency and maximum velocity and also possesses the proper shape of the frequency-responsefunction. Note that two resonance frequencies are predicted by the lumped element model, one near 350 Hz and the other near 900 Hz. However, the lower peak is heavily damped in Fig. 12 due to the frequency-dependent nonlinear orifice resistance term $R_{aO}(\omega)$. An inspection of Eqs. (4) and (5) reveals that this term has a larger effect at lower frequencies. Gallas et al.[30] mistakenly argued that this case corresponds to the situation when a single peak is obtained in the frequency-response function $f_1 = f_2 = \sqrt{(f_D f_H)}$.

Finally, the peak in the experimental results for case 2, which occurs at around 1200 Hz, corresponds to a harmonic of the resonance frequency of the piezoelectric diaphragm. The lumped element model does not account for structural nonlinearities or higher-order vibration modes. As a result, the peak near 1200 Hz is not captured by the model.

V. Conclusions

A lumped element model of a piezoelectric-driven synthetic-jet actuator has been developed and compared with experiment. LEM provides a compact analytical model and valuable physical insight into the dependence of the device behavior on geometry and material properties. The model reveals that a synthetic jet is a fourth-order coupled oscillator. One oscillator is a Helmholtz resonator, and the second is the piezoelectric diaphragm. Simple arguments reveal two important special cases corresponding to single oscillators. One case occurs when the flow is incompressible, whereas the second case is similar to that of a rigid piston and occurs when the acoustic compliance of the piezoelectric diaphragm is small compared to that of the cavity. In this case, the synthetic jet acts like a driven Helmholtz resonator. For any case with low damping, which is found to be a reasonable assumption, a simple formula was obtained to estimate the two natural frequencies of the synthetic jet as a function of the Helmholtz and diaphragm natural frequencies and the compliance ratio β.

Methods to estimate the parameters of the lumped element model were presented and experiments were performed to isolate different components of the model and evaluate their suitability. The results indicate that the linear composite plate theory is accurate when the model assumptions are achieved, that is, linear response, clamped boundary condition, negligible bond layer, and no in-plane stress. Similarly, the cavity acoustic compliance model was validated. The details of the flow in the orifice require a careful study. It is this region that dictates the acoustic mass and resistance in the neck. Accurate knowledge of the acoustic mass is required to determine the Helmholtz frequency of the synthetic jet, whereas the resistance limits the achievable velocities near resonance.

The model was applied to two prototypical synthetic jets and found to provide very good agreement with the measured performance. The only adjustable constant is the structural damping

coefficient, which affects the results near the diaphragm resonance frequency. The results reveal the power and shortcomings of the model in its present form. The flow in the vicinity of the orifice must be studied further to obtain better quantitative estimates of the losses and velocity profile characteristics. Furthermore, the loss coefficient K_D in Eq. (32) is assumed to be unity, but is probably a function of the orifice Reynolds number, Stokes number, and geometry, for example, a rounded orifice. Furthermore, grazing flow effects remain to be studied in a rigorous fashion.

In future work, additional parameters will be varied in the model and accompanying experiments to yield optimal design rules for the synthetic jet. Future testing of the piezoelectric diaphragm will assess the severity of nonlinear effects when the excitation amplitude is increased, as well as the impact of the edge boundary condition on the diaphragm performance. For the orifice, emphasis will be placed on the ratio of the orifice length to the hole radius L/a_0. This variable will be systematically varied in concert with the other important parameters, such as the orifice shape, Reynolds, and Stokes numbers. Additional velocity measurements with improved spatial resolution will also be performed to map out the spatial variations in the synthetic-jet velocity field.

Acknowledgments

The authors gratefully acknowledge grant support from NASA Langley Research Center (monitored by S. Gorton) and the U.S. Air Force Office of Scientific Research (monitored by J. Schmisseur). The authors are grateful to B. Sankar, S. Horowitz, J. Mathew, A. Kasyap, and S. Prasad for their contributions to this paper and also thank M. Kegerise and R. Mittal for many insightful discussions.

References

[1]Smith, B. L., and Glezer, A., "The Formation and Evolution of Synthetic Jets," *Physics of Fluids*, Vol. 10, No. 9, 1998, pp. 2281–2297.

[2]Amitay, M., Smith, B. L., and Glezer, A., "Aerodynamic Flow Control Using Synthetic Jet Technology," AIAA Paper 98-0208, Jan. 1998.

[3]Smith, D. R., Amitay, M., Kibens, V., Parekh, D. E., and Glezer, A., "Modification of Lifting Body Aerodynamics Using Synthetic Jet Actuators," AIAA Paper 98-0209, Jan. 1998.

[4]Chen, Y., Liang, S., Aung, K., Glezer, A., and Jagoda, J., "Enhanced Mixing in a Simulated Combustor Using Synthetic Jet Actuators," AIAA Paper 99-0449, Jan. 1999.

[5]Honohan, A. M., Amitay, M., and Glezer, A., "Aerodynamic Control Using Synthetic Jets," AIAA Paper 2000-2401, June 2000.

[6]Chatlynne, E., Rumigny, N., Amitay, M., and Glezer, A., "Virtual Aero-Shaping of a Clark-Y Airfoil Using Synthetic Jet Actuators," AIAA Paper 2001-0732, Jan. 2001.

[7]Crook, A., Sadri, A. M., and Wood, N. J., "The Development and Implementation of Synthetic Jets for the Control of Separated Flow," AIAA Paper 99-3176, July 1999.

[8]Chen, F.-J., Yao, C., Beeler, G. B., Bryant, R. G., and Fox, R. L., "Development of Synthetic Jet Actuators for Active Flow Control at NASA Langley," AIAA Paper 2000-2405, June 2000.

[9]Crook, A., and Wood, N. J., "Measurements and Visualizations of Synthetic Jets," AIAA Paper 2001-0145, Jan. 2001.

[10]Gilarranz, J. L., and Rediniotis, O. K., "Compact, High-Power Synthetic Jet Actuators for Flow Separation Control," AIAA Paper 2001-0737, Jan. 2001.

[11]Kral, L. D., Donovan, J. F., Cain, A. B., and Cary, A. W., "Numerical Simulation of Synthetic Jet Actuators," AIAA Paper 97-1824, June 1997.

[12]Rizzetta, D. P., Visbal, M. R., and Stanek, M. J., "Numerical Investigation of Synthetic Jet Flowfields," AIAA 98-2910, June 1998.

[13]Mallinson, S. G., Reizes, J. A., Hong, G., and Haga, H., "The Operation and Application of Synthetic Jet Actuators," AIAA Paper 2000-2402, June 2000.

[14]Utturkar, Y., Mittal, R., Rampunggoon, P., and Cattafesta, L., "Sensitivity of Synthetic Jets to the Design of the Jet Cavity," AIAA Paper 2002-0124, Jan. 2002.

[15]Fischer, F. A., *Fundamentals of Electroacoustics*, Interscience, New York, 1955, Chaps. 3 and 11.

[16]Merhaut, J., *Theory of Electroacoustics*, McGraw–Hill, New York, 1981, Chap. 6.

[17]Rossi, M., *Acoustics and Electroacoustics*, Artech House, Norwood, MA, 1988, pp. 245–373.

[18]McCormick, D. C., "Boundary Layer Separation Control with Directed Synthetic Jets," AIAA Paper 2000-0519, Jan. 2000.

[19]Rathnasingham, R., and Breuer, K. S., "Coupled Fluid-Structural Characteristics of Actuators for Flow Control," *AIAA Journal*, Vol. 35, No. 5, 1997, pp. 832–837.

[20]Prasad, S., Horowitz, S., Gallas, Q., Sankar, B., Cattafesta, L., and Sheplak, M., "Two-Port Electroacoustic Model of an Axisymmetric Piezoelectric Composite Plate," AIAA Paper 2002-1365, April 2002.

[21]Sheplak, M., Schmidt, M. A., and Breuer, K. S., "A Wafer-Bonded, Silicon Nitride Membrane Microphone with Dielectrically-Isolated, Single-Crystal Silicon Piezoresistors," Technical Digest, Solid-State Sensor and Actuator Workshop, Hilton Head, SC, 1998, pp. 23–26.

[22]Beranek, L. L., *Acoustics*, Acoustic Society of America, Woodbury, NY, 1993, pp. 47–77, 116–143.

[23]Blackstock, D. T., *Fundamentals of Physical Acoustics*, Wiley, New York, 2000, p. 145.

[24]White, F. M., *Fluid Mechanics*, McGraw–Hill, New York, 1979, pp. 377–379.

[25]White, F. M., *Viscous Flow*, McGraw–Hill, New York, 1974, pp. 143–148.

[26]Bendat, J. S., and Piersol, A. G., *Random Data: Analysis and Measurements Procedures*, 3rd ed., Wiley, New York, 2000, p. 341.

[27]Ingard, U., *Notes on Sound Absorbers*, Kittery Point, ME, 1999, p. 80 (self-published), URL: http://www.ingard.com.

[28]Ingard, U., "Acoustic Nonlinearity of an Orifice," *Journal of Acoustic Society of America*, Vol. 42, No. 1, 1967, pp. 6–17.

[29]Mittal, R., Rampuggoon, P., and Udaykumar, H. S., "Interaction of a Synthetic Jet with a Flat Plate Boundary Layer," AIAA Paper 2001-2773, June 2001.

[30]Gallas, Q., Mathew, J., Kaysap, A., Holman, R., Carroll, B., Nishida, T., Sheplak, M., and Cattafesta, L., "Lumped Element Modeling of Piezoelectric-Driven Synthetic Jet Actuators," AIAA Paper 2002-0125, Jan. 2002.

M. Ahmadian
Associate Editor